

Evidence for Mature Bulges and an Inside-out Quenching Phase 3 Billion Years After the Big Bang

Authors: S. Tacchella^{1*}, C. M. Carollo^{1*}, A. Renzini², N. M. Förster Schreiber³, P. Lang³, S. Wuyts³, G. Cresci⁴, A. Dekel⁵, R. Genzel^{3,6,7}, S. J. Lilly¹, C. Mancini², S. Newman⁶, M. Onodera¹, A. Shapley⁸, L. Tacconi³, J. Woo¹, & G. Zamorani⁹

Affiliations:

¹Department of Physics, Institute for Astronomy, ETH Zurich, CH-8093 Zurich, Switzerland

²INAF Osservatorio Astronomico di Padova, vicolo dell Osservatorio 5, I-35122 Padova, Italy

³Max-Planck-Institut für extraterrestrische Physik (MPE), Giessenbachstr. 1, D-85748 Garching, Germany

⁴Istituto Nazionale di Astrofisica – Osservatorio Astronomico di Arcetri, Largo Enrico Fermi 5, I-50125 Firenze, Italy

⁵Racah Institute of Physics, The Hebrew University, Jerusalem 91904, Israel

⁶Department of Astronomy, Campbell Hall, University of California, Berkeley, CA 94720, USA

⁷Department of Physics, Le Conte Hall, University of California, Berkeley, CA 94720, USA

⁸Department of Physics and Astronomy, University of California, Los Angeles, CA 90095-1547, USA

⁹INAF Osservatorio Astronomico di Bologna, Via Ranzani 1, I-40127 Bologna, Italy

* sandro.tacchella@phys.ethz.ch; marcella.carollo@phys.ethz.ch

Most present-day galaxies with stellar masses $\geq 10^{11}$ solar masses show no ongoing star formation and are dense spheroids. Ten billion years ago, similarly massive galaxies were typically forming stars at rates of hundreds solar masses per year. It is debated how star formation ceased, on which timescales, and how this ‘quenching’ relates to the emergence of dense spheroids. We measure stellar mass and star-formation rate surface density distributions in star-forming galaxies at redshift 2.2 with ~ 1 kpc resolution. We find that, in the most massive galaxies, star-formation is quenched from the inside out, on timescales < 1 Gyr in the inner regions, up to a few Gyr in the outer disks. These galaxies sustain high star-formation activity at large radii, while hosting fully grown and already quenched bulges in their cores.

At the epoch when star-formation activity peaks in the Universe (redshift $z \sim 2$; *1, 2*), massive galaxies typically lie on the so-called ‘star-forming main sequence’. Their star-formation rates (SFRs) tightly correlate with the mass in stars (stellar mass *M*), reaching up to

several hundred $M_{\odot} \text{ yr}^{-1}$ (where M_{\odot} is the mass of the sun) and producing a characteristic specific SFR ($\text{sSFR}=\text{SFR}/M$) that declines only weakly with mass (e.g., 3, 4). In contrast, at the present epoch, such massive galaxies are spheroids with old stellar populations, which reach central surface stellar densities well above $10^{10} M_{\odot} \text{ kpc}^{-2}$ and host virtually no ongoing star-formation. While the most massive ellipticals at $z=0$ bear the clear signatures of a gas-poor formation process (5, 6), the more typical population, at a mass scale of $M\sim 10^{11} M_{\odot}$, consists of fast rotators (7) with disk-like isophotes (8), steep nuclear light profiles (9) and steep metallicity gradients (10) – all features that indicate a gas-rich formation process.

The full cessation of star-formation activity in these typical massive galaxies (here referred to as the quenching process) is not well understood, nor is its relation with the emergence of their spheroidal morphologies. Several quenching mechanisms have been proposed. The so-called halo-quenching scenario predicts that circumgalactic gas is shock-heated to high temperatures and stops cooling in dark matter halos above a critical mass ($\sim 10^{12} M_{\odot}$; 11). Morphological/gravitational quenching proposes that the growth of a central mass concentration, i.e., a massive bulge, stabilizes a gas disk against fragmentation (12, 13). Feedback from an accreting supermassive black hole transfers either radiative (14) or kinetic energy and momentum (15) to the surrounding gas, respectively, expelling gas from the galaxy or suppressing gas accretion onto it.

Quenching must soon occur in the most massive – and thus formidably star-forming – galaxies on the main sequence at $z\sim 2$, to avoid dramatically overshooting the highest observed masses of $z=0$ galaxies (16). Yet, no general consensus has emerged on which of the above mentioned processes is primarily responsible for halting this star formation as early as a few Gyrs after the Big Bang. Determining the distributions of the stellar mass and SFR densities within individual $z\sim 2$ galaxies at high spatial resolution is central to resolving these issues. Together these distributions reveal how stellar mass builds up and SFR is progressively switched off inside these high- z galaxies which, given their high masses, will have to evolve into ‘red and dead’ systems by $z=0$.

We measured such quantities for a sample of 22 star-forming galaxies at a median redshift of 2.2 (see 17 and Section S1). The sample spans a wide range in stellar mass $M\sim 4\cdot 10^9\text{--}5\cdot 10^{11} M_{\odot}$ and $\text{SFR}\sim 20\text{--}300 M_{\odot} \text{ yr}^{-1}$, and broadly traces the main sequence at these redshifts.

The five most massive galaxies lie slightly below the average main sequence, a point we explore in more detail in Section S1.

For all galaxies we obtained adaptive-optics SINFONI (Spectrograph for INtegral Field Observations in the Near Infrared) spectroscopy on the European Southern Observatory’s Very Large Telescope, mapping the two-dimensional rest-frame H α emission at ~ 1 kpc spatial resolution. These data reflect the gas ionized by young stars within individual galaxies which allows us to construct spatially resolved distributions of ionized gas kinematics and SFR surface densities internal to the galaxy. We also obtained Hubble Space Telescope (HST) imaging in the J and H passbands (17, 18). At the redshifts of the sample, the J and H filters straddle the rest-frame Balmer/4000Å-break. This spectral feature is strong in relatively old stars and therefore provides a robust estimate of the stellar mass already assembled in older stellar populations. Thus, at a similar \sim kpc resolution as the SINFONI SFR maps, the HST images provide maps of the stellar mass density that is stored in such older underlying populations. Visual inspection of the two-dimensional SFR distributions immediately reveals their notoriously irregular appearance, with bright clumps at large radii, in contrast with their centrally peaked and smooth stellar mass distributions (Figs. S4-S6).

The shapes of the average surface SFR density (Σ_{SFR}) profiles (Fig. 1, top panels) are very similar regardless of total mass and are well fitted by a Sérsic profile $\Sigma \propto \exp(-\beta \cdot r^{1/n})$, with the $n \sim 1$ value typical of disk-like systems. In contrast, the surface stellar mass density (Σ_{M}) profiles become progressively more centrally concentrated with increasing total stellar mass. The Sérsic index of the Σ_{M} profiles increases from $n=1.0 \pm 0.2$ in the low mass bin, to $n=1.9 \pm 0.6$ in the intermediate mass bin, up to $n=2.8 \pm 0.3$ in the high mass bin (uncertainties indicate the 1σ scatter). Within each mass bin, the mean Σ_{M} profiles are always more centrally concentrated than the SFR density profiles.

We then compared the Σ_{M} profiles of our sample of $z \sim 2.2$ galaxies with a mass-matched sample of local $z=0$ galaxies (Fig. 1, bottom panels; 19). Consistently with the Sérsic fits, the low-mass $z \sim 2.2$ galaxies have the same radial stellar mass profiles of late-type disks in the local Universe. The $z \sim 2.2$ galaxies in the most massive bin, however, have stellar mass profiles that overlap with those of $z=0$ early-type galaxies out to galactocentric distances of a few kpc, corresponding to typically ~ 2 effective radii. At these high stellar masses ($\sim 10^{11} M_{\odot}$), our sample

of galaxies on the $z \sim 2.2$ have therefore already saturated their central stellar mass densities to those of galaxies of similar mass at $z=0$, which are quenched systems with a bulge-dominated morphology. Thus, the bulge components of these massive galaxies are already fully in place while their hosts are still vigorously forming stars further out in the surrounding (disk) regions (Figs. 1 & 2, center panels; see also 13).

Specifically, the ratio between the star formation rate and stellar mass surface density profiles, i.e., $sSFR_r = \Sigma_{SFR}(r)/\Sigma_M(r)$, indicates suppression of the inner $sSFR_r$ at the highest masses and generally outwards-increasing radial profiles of $sSFR_r$ (Fig. 1, center panels). By examining the surface stellar mass density within 1 kpc, $\Sigma_{M,1kpc}$, as a function of total stellar mass M , we see that the massive galaxies at $z \sim 2.2$ in our sample have substantially suppressed star formation activity in their centers relative to lower-mass galaxies at the same epochs. We show in the supplementary materials (17) that this cannot be entirely due to dust effects. The $sSFR_{1kpc}$ values range from $sSFR_{1kpc} \sim 5 \text{ Gyr}^{-1}$ (corresponding to a mass doubling time of $\sim 200 \text{ Myr}$ at a galaxy stellar mass of $10^{10} M_\odot$) down to negligible values of $\sim 0.1 \text{ Gyr}^{-1}$ at $10^{11} M_\odot$. The key conclusion is therefore that these galaxies sustain their high total SFRs at large radii, far from their central dense cores, whereas in such cores the $sSFR_r$ is about two orders of magnitude lower.

A further important consideration that emerges from the analysis of Fig. 2 is that our galaxies lie around the identical, tight $\Sigma_{M,1kpc}$ - M sequence that is traced by galaxies at $z \sim 0$ (20). This implies that the increase in total M of individual galaxies along the main sequence must be accompanied by a synchronized increase in central $\Sigma_{M,1kpc}$ – until the maximal central stellar densities of today’s massive spheroids are reached at a stellar mass scale of order $\sim 10^{11} M_\odot$. Below this galaxy mass scale, dense stellar bulges are therefore built concurrently with the outer galactic regions. At $z=0$, the global relation curves because the quenched galaxies have a shallower slope than the star-forming galaxies, and a clear ‘ridge’ emerges (Fig. 2 ; 21). We have too few galaxies to track this curvature at earlier times, but this trend would be consistent with $z \sim 2.2$ galaxies slightly increasing their total M through declining star-formation at large radii while maintaining their already quenched inner $\Sigma_{M,1kpc}$ values.

These results provide insight into the bulge formation process. The high stellar densities that are already present in their cores indicate that at least some massive star-forming galaxies at

$z \sim 2.2$ have today's massive spheroids as their descendants. We are seeing however neither 'classical bulges' formed by dissipationless merging, nor 'pseudo-bulges' formed by the slow, secular evolution of a stellar disk. Such a dichotomy is often invoked to explain the structural variety observed in nearby galactic bulges (22, see however 23). The high central stellar densities of the massive galaxies in our sample argue for a gas-rich, dissipative bulge formation process at even earlier epochs. This is consistent with theoretical predictions (24), that either mergers or violent disk instabilities in gas-rich galactic structures at high redshifts lead to a 'compaction' phase of the gas component, which possibly even drags any pre-existing stellar component within the inner few kpc.

Furthermore, the suppressed central sSFRs in such massive systems argue for a 'quenching engine' also at work. As this apparently acts from the inner galactic regions outwards, it echoes findings recently reported for massive galaxy populations in a more recent era, at $z \sim 0.5-1.5$, or $\sim 1.5-5.5$ Gyr later (25, 26). Our results reveal that similar signatures are seen as early as $z \sim 2.2$, implying that the same physical processes that lead to a phase of suppressed star formation from the inside-out start acting on massive star-forming galaxies as early as ~ 3 Gyr after the Big Bang. We also estimate the time scale for an inside-out 'quenching wave' to propagate across $\sim 10^{11} M_{\odot}$ galactic bodies (Fig. 3). The estimate assumes that our galaxies keep forming stars with their observed radial profiles of surface SFR density, until their $\Sigma_M(r)$ reaches the value observed in $z=0$ passive galaxies of similar stellar mass. This allows quenching timescales substantially less than 1 Gyr in the galaxy centers and roughly 3 billion years in the outer disk/ring regions. These give rise to a stellar age gradient of $d \log(\text{age})/d \log(r) \sim -0.5$ dex per radial decade (see 17). This predicted age gradient in the stellar population implies a negative color gradient in passive $z \sim 1-2$ spheroids, which is found in several studies (27, 28); with flat metallicity gradients, the inferred average age gradients range between about -0.1 and -0.4 dex per radial decade. A contribution to the color gradient from either dust or metallicity effects would imply that such estimates are lower limits to such photometrically-estimated stellar age. The galaxies will be fully quenched by $z \sim 1$; subsequent passive evolution down to $z=0$ will produce quenched $z=0$ remnants with the 'dissipative' properties of typical $\sim M^*$ spheroids, such as disk-like isophotes and fast-rotating kinematics (Fig. 4).

Our results also provide insight into quenching mechanisms. Clearly an external process such as a large-scale shutdown of gas supply caused by a hot halo or a low cosmological

accretion rate may still contribute to inside-out quenching. The fact that we observe a phase of inside-out quenching in very massive galaxies at early epochs suggests however also a prominent role of an internal process operating from the inner galaxy regions. The most massive galaxies in our sample exhibit fast, nuclear outflows, which may indeed signify that active galactic nuclei feedback is also a factor (29). By setting the condition for sustainment of star-formation, the local stellar density within galaxies may also be acting as the internal process that regulates the rate at which SFR is locally suppressed (30). The current analysis cannot identify the direction of the causality between the presence of a high stellar mass density and the cessation of star-formation, but it is clear from our data that such high stellar density is present when quenching starts. Our study therefore highlights either, or possibly both, of these two internal processes as a key contributor to the downfall of the most massive and most star-forming galaxies at the peak of galaxy formation.

References and Notes:

1. S. J. Lilly, L. Tresse, F. Hammer, D. Crampton, O. Le Fevre, *ApJ* **455**, 108 (1995)
2. P. Madau, *et al.*, *MNRAS* **283**, 1388 (1996)
3. K. J. Noeske, *et al.*, *ApJL* **660**, 43 (2007)
4. E. Daddi, *et al.*, *ApJ* **670**, 156 (2007)
5. T. Naab, A. Burkert, *ApJ* **597**, 893 (2003)
6. T. J. Cox, *et al.*, *ApJ* **650**, 791 (2006)
7. M. Cappellari, *et al.*, *MNRAS* **379**, 418 (2007)
8. R. Bender, S. Doebereiner, C. Moellenhoff, *A&AS* **74**, 385 (1988)
9. S. M. Faber, *et al.*, *AJ* **114**, 1771 (1997)
10. C. M. Carollo, I. J. Danziger, L. Buson, *MNRAS* **265**, 553 (1993)
11. A. Dekel, Y. Birnboim, *MNRAS* **368**, 2 (2006)
12. M. Martig, F. Bournaud, R. Teyssier, A. Dekel, *ApJ* **707**, 250 (2009)
13. R. Genzel, *et al.*, *ApJ* **785**, 75 (2014)

14. T. Di Matteo, V. Springel, L. Hernquist, *Nature* **433**, 604 (2005)
15. D. J. Croton, *et al.*, *MNRAS* **365**, 11 (2006)
16. A. Renzini, *MNRAS* **398**, 58 (2009)
17. Materials and methods are available as supplementary materials on Science Online.
18. S. Tacchella, *et al.*, (2014), *ApJ*, submitted (available at arxiv.org/abs/1411.7034)
19. C. M. Carollo, *et al.*, *ApJ* **776**, 71 (2013)
20. P. Saracco, A. Gargiulo, M. Longhetti, *MNRAS* **422**, 3107 (2012)
21. J. J. Fang, S. M. Faber, D. C. Koo, A. Dekel, *ApJ* **776**, 63 (2013)
22. J. Kormendy, R. C. Jr. Kennicutt, *ARAA* **42**, 603 (2004)
23. C. M. Carollo, C. Scarlata, M. Stiavelli, R. F. G. Wyse, L. Mayer, *ApJ* **658**, 960 (2007)
24. A. Dekel & A. Burkert, *MNRAS* **438**, 1870 (2014)
25. E. J. Nelson, *et al.*, *ApJL* **763**, L16 (2013)
26. S. Wuyts, *et al.*, *ApJ* **779**, 135 (2013)
27. Y. Guo, *et al.*, *ApJ* **735**, 18 (2011)
28. A. Gargiulo, *et al.*, *MNRAS* **425**, 2698 (2012)
29. N. M. Förster Schreiber, *et al.*, *ApJ* **787**, 38 (2014)
30. J. Woo, A. Dekel, S. M. Faber, D. C. Koo, *MNRAS* **448**, 237 (2015)

Acknowledgments:

ST thanks B. Trakhtenbrot for stimulating discussions. We thank the reviewers for their thorough review, their comments and suggestions. We acknowledge support by the Swiss National Science Foundation, grant #200020_140952. This research made use of NASA's Astrophysics Data System, the arXiv.org preprint server, the Python plotting library matplotlib, and astropy, a community-developed core Python package for Astronomy. AR, GC and GZ acknowledge support from a INAF 'PRIN-2012'. Based on observations made with the NASA/ESA Hubble Space Telescope, obtained at the Space Telescope Science Institute, which is operated by the

Association of Universities for Research in Astronomy, Inc., under NASA contract NAS 5-26555 and on observations obtained at the Very Large Telescope of the European Southern Observatory, Paranal, Chile. The data used in this paper archived at <https://archive.stsci.edu/hst/> under program ID GO9822, GO10092, GO10924, GO11694, GO12578, GO12060, GO12061, GO12062, GO12063, GO12064, GO12440, GO12442, GO12443, GO12444, and GO12445; and <http://archive.eso.org> under program ID 075.A-0466, 076.A-0527, 079.A-0341, 080.A-0330, 080.A-0339, 080.A-0635, 081.A-0672, 183.A-0781, 087.A-0081, 088.A-0202, 088.A-0209, and 091.A-0126.

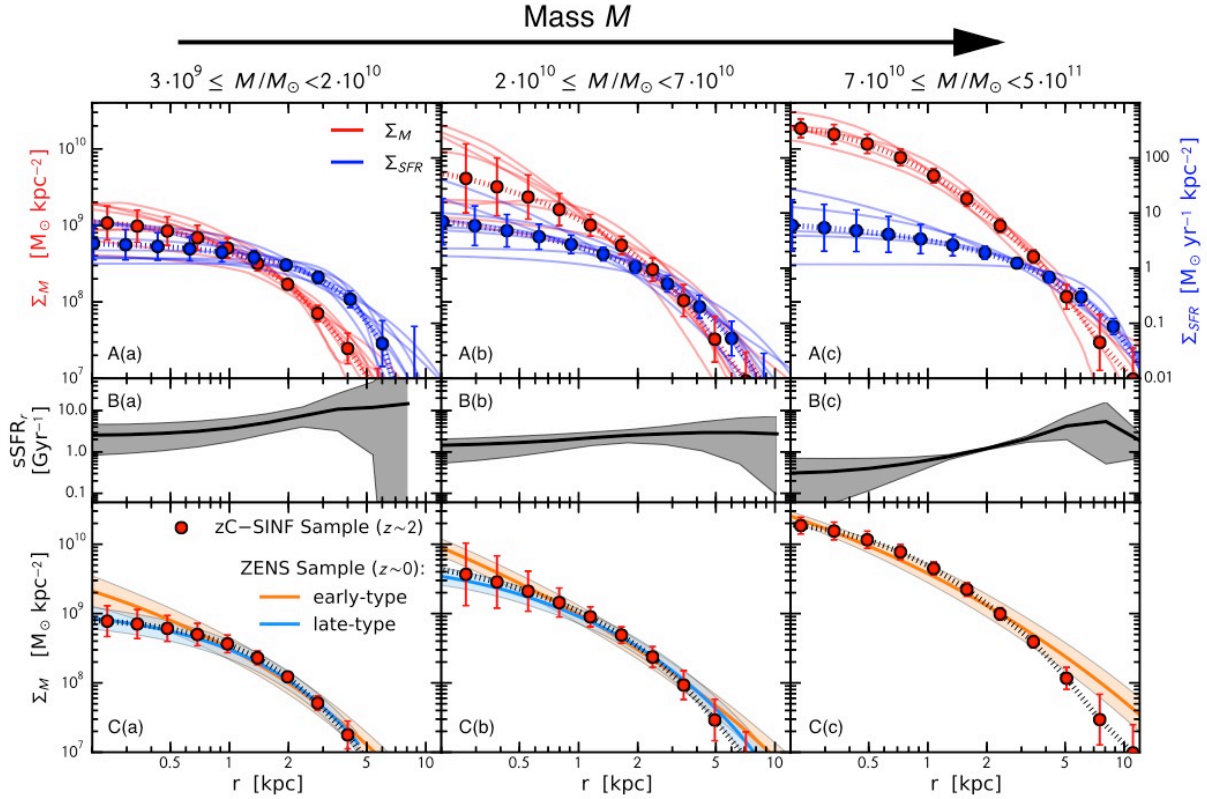


Fig. 1. Stellar mass and star-formation rate surface density distributions. The three columns of panels (a-c) show results for the three bins of stellar mass indicated at the top of each column containing 9, 8, and 5 galaxies, respectively. Upper row (A): The stellar surface mass density profiles (red, scale on the left vertical axis) and SFR surface density profiles (blue, scale on the right vertical axis) for our $z \sim 2.2$ sample. Thin lines represent individual galaxies; the mean values are given by the filled circles (with error bars indicating the 1σ scatter). The derivation of these profiles are described in detail in the supplementary materials (17). Middle row (B): The mean sSFR as a function of radius r ($sSFR_r$; black line). In gray we show the 1σ scatter. Bottom row (C): The average surface stellar mass density profiles of the star-forming $z \sim 2.2$ galaxies (red points with dashed line; error bars indicate the 1σ scatter) overplotted on the average profiles for the mass-matched samples of $z=0$ galaxies (colors indicating morphological types: orange for early-types, blue for late-types).

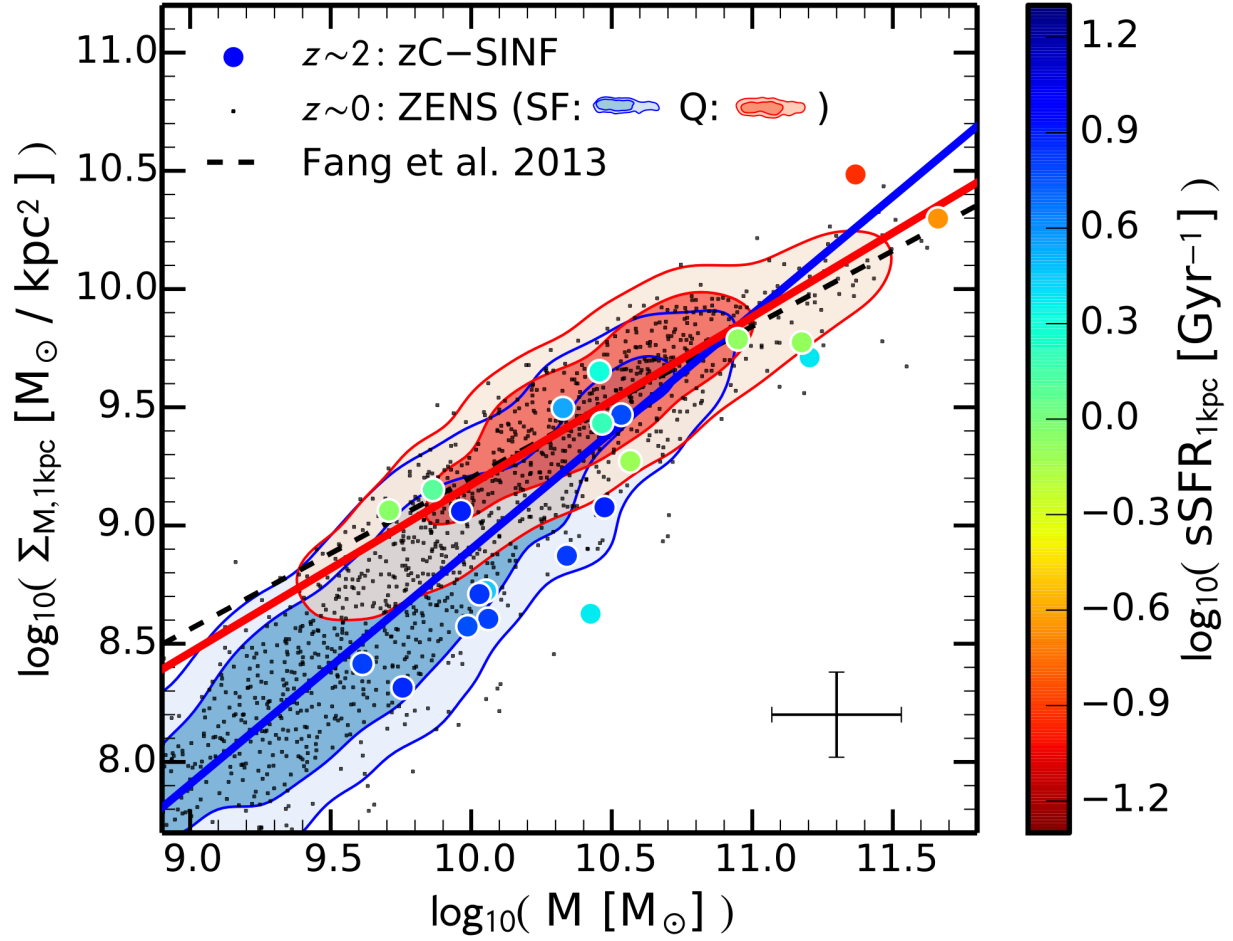


Fig. 2. Central stellar mass density sequence. We plot the stellar mass surface density within 1 kpc, $\Sigma_{M,1\text{kpc}}$, as a function of the total stellar mass M . The black points show the $z\sim 0$ ZENS sample, and the blue and red contours their density on the $\Sigma_{M,1\text{kpc}}-M$ plane split for star-forming (blue) and quiescent (red) galaxies. The correspondingly-colored solid lines indicate the best fits to these $z=0$ star-forming ($\Sigma_{M,1\text{kpc}} \propto M^{-1.0}$) and quiescent ($\Sigma_{M,1\text{kpc}} \propto M^{-0.7}$) galaxies. The dashed black line shows the fit to the ‘ridge’ of passive galaxies in the SDSS $z=0$ sample of Fang et al. (20). The error bar in the bottom-right indicate the systematic uncertainty in the derivation of $\Sigma_{M,1\text{kpc}}$ and M . The large points are the $z\sim 2.2$ galaxies, color-coded according to specific star-formation rate within 1 kpc, $s\text{SFR}_{1\text{kpc}}$. The $z\sim 2.2$ galaxies lie on the tight $\Sigma_{M,1\text{kpc}}-M$ locus traced by the $z=0$ population. In contrast with total SFRs increasing with stellar mass along the ‘main sequence’, the $z\sim 2.2$ galaxies have central sSFRs that strongly decrease with stellar mass.

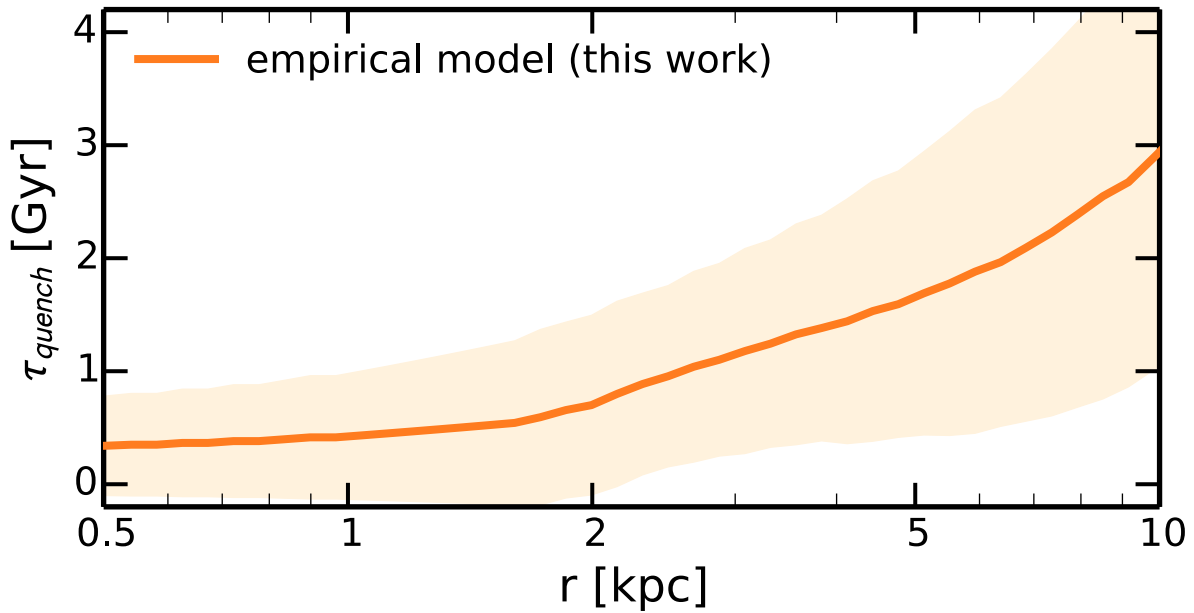


Fig. 3. Outward progression of the quenching wave. The quenching time τ_{quench} in star-forming $\sim 10^{11} M_{\odot}$ galaxies at $z \sim 2.2$ as a function of galactocentric distance. Such galaxies quench inside-out on time scales in the inner cores much shorter than 1 Gyr after observation, up to a few Gyr in the galactic peripheries. The galaxies will be fully quenched by $z \sim 1$. The solid orange line indicates the mean quenching time for all galaxies in the highest mass bin, while the orange-shaded region marks the 1σ scatter.

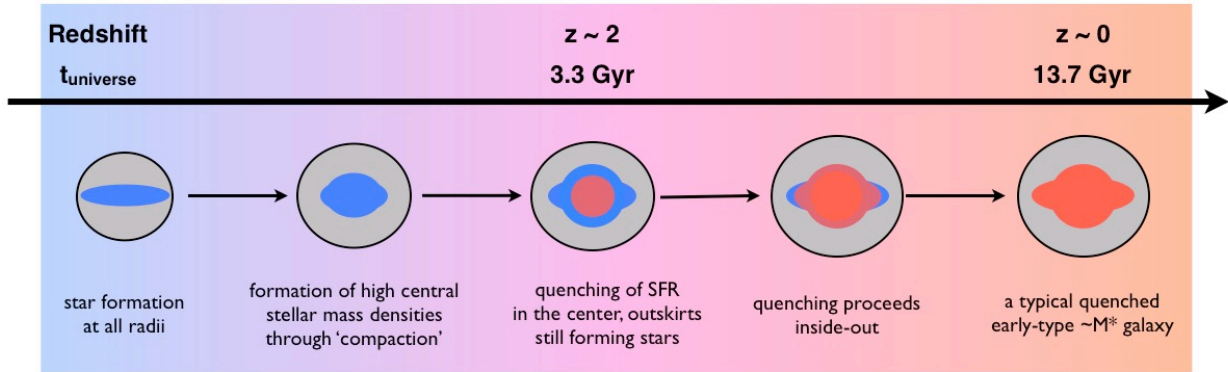


Fig. 4. Proposed sketch for the evolution of massive galaxies. Our results suggest a picture in which the total stellar mass and bulge mass grow synchronously in $z \sim 2$ main sequence galaxies, and quenching is concurrent with their total masses and central densities approaching the highest values observed in massive spheroids in today's Universe.